

Developing a Dual Polarization Antenna (DPA) for High Dynamic Applications

Sherman Lo, *Stanford University*, Yu Hsuan Chen, *Stanford University*, Fabian Rothmaier, *Stanford University*, Godwin Zhang, *Stanford University*, Chiawei Lee, *US Air Force Test Pilot School*

BIOGRAPHIES

Sherman Lo is a senior research engineer at the Stanford GPS Laboratory. He received his Ph.D. in Aeronautics and Astronautics from Stanford University in 2002. He has and continues to work on navigation robustness and safety, often supporting the FAA. He has conducted research on Loran, alternative navigation, SBAS, ARAIM, GNSS for railways and automobile. He also works on spoof and interference mitigation for navigation. He has published over 100 research papers and articles. He was awarded the ION Early Achievement Award.

Yu-Hsuan Chen is a research engineer at the Stanford GPS Laboratory. He received his Ph.D. in Electrical Engineering from National Cheng Kung University, Taiwan in 2011.

Fabian Rothmaier is a PhD candidate at the GPS Laboratory at Stanford University. He received his B. Engr. degree from the University of Applied Sciences Bremen, Germany in 2015 and his M. Sc. degree from Stanford University in 2017.

Godwin Zhang is a research engineer in the Department of Aeronautics & Astronautics.

Chiawei Lee is an Instructor Flight Test Engineer at the US Air Force Test Pilot School where he is primarily responsible for Test Management Projects. He earned his MS in Aero/Astro Engineering from Stanford University and BS in Aerospace Engineering from UCLA.

ABSTRACT

GNSS spoofing is a growing concern due to the increasing use of GNSS in safety and economically important applications. The foremost task to manage GNSS spoofing is detection. Indeed, many potential means and measurements have been proposed for spoof detection but there are no panaceas. One measurement that is both useful for detection and independent of other metrics is direction of arrival (DOA). One way to get DOA is using a dual polarization antenna (DPA). While we can get DOA from more specialized antennas such as directional and array antennas, the DPA can offer this capability with a single patch antenna. Stanford has developed a prototype DPA using only commercial off the shelf (COTS) parts that has demonstrated the ability to determine direction. However, for the developed prototype to be practical, especially for high dynamic applications such as flight, the DOA determination needs to be faster and preferably more accurate. This paper examines our development to improve DOA determination time. Two approaches are used. First, a software defined radio (SDR) is developed to improve the DPA DOA determination time, reducing the minute long determination to near instantaneous. The paper examines the development and testing of SDR processing of DPA measurements for DOA determination. However, the cost of this approach is specialized dedicated hardware and additional processing which will be detailed in the paper. Hence the paper also examines improvements to our COTS design hardware to speed up DOA determination. DOA determination at about 0.5 Hz was demonstrated using an improved COTS design.

INTRODUCTION

Dual polarization antennas (DPAs) are being developed to provide robust GNSS spoof detection. The technology shows great potential in determining the direction of arrival (DOA) of incoming GNSS signals with just a single GNSS patch antenna. While the Stanford prototype version of the DPA has demonstrated these capabilities but it also has some important limitations that must be overcome to make DPA a practical general purpose spoof detection technique. Specifically, Stanford

DPA should be able to find DOAs rapidly and more accurately. These improvements may be enabled with architecture change and demonstrated using a commercial off the shelf (COTS) GNSS receiver and a software defined radio (SDR).

DPA determines direction of arrival (DOA) by comparing right and left hand circularly polarized (RHCP, LHCP, respectively). By DOA, we mean the direction of arrival relative to the x-axis (top) of the antenna. While GNSS signals are typically RHCP, any signal impacting the ground plane prior to entering the antenna will develop LHCP components and the relationship of this component with the RHCP is related to the direction of arrival. By finding the phase relationship between the two signals, the direction of arrival can be determined, though with a 180 degree ambiguity.

Field trials have demonstrated the capability of the DPA in finding incoming DOAs of both genuine and spoofed GNSS signals. The set up in [1] used a printed circuit board (PCB) based DPA with a hybrid coupler to create the RHCP and LHCP measurements. These measurements are combined using a phase shifter and processed with a commercial GNSS receiver (application specific) integrated circuit (ASIC/IC) to find the phase offset between RHCP and LHCP. While this allowed for low cost and lightweight implementation, the approach is limited as this is a serial search process for the phase offset and the unit used in the field exercises in reference [2] required 50-250 seconds to find DOAs. Several solutions are possible and will be discussed in the paper. One solution is to improve our COTS GNSS IC based design. Another is to employ a SDR receiver approach, which allows for parallel processing of the measurements and give a DOA estimate with each measurement taken. The SDR approach may also have other benefits for DOA accuracy and interference mitigation.

This paper describes the improved DPA for high dynamic applications. Primarily, it examines two approaches (GNSS IC and SDR) for fast DOA estimates. It will detail the designed and implemented architectures for rapid DOA estimates with both approaches. It also discusses the SDR approach for processing DPA for interference mitigation. The paper then demonstrates the performance of each approach by building real time hardware to gather data from on air tests. This equipment is made suitable for installation on an aircraft and used in a flight test program in partnership with the US Air Force Test Pilot School. Earlier, static and inertial augmented dynamic results with this antenna was published in [3] and this paper will examine new results based on dynamic flight tests.

BACKGROUND

Dual Polarization Antenna

GNSS dual polarization antennas can simultaneously provide the antenna reception of two different polarization. This can be built on a standard patch using two appropriately placed feeds [4]. These feeds are typically chosen so that they output the response of the antenna to two orthogonal linearly polarized signals. The signals from each feed, denoted as being x- and y-axis, are shown in Figure 1. Figure 2 shows that these signals are sent to a 90 degree hybrid coupler to generate RHCP and LHCP signals. Such antennas have been around for some time and have been proposed for use to mitigate interference, particularly as part of a controlled reception pattern array (CRPA) where they can provide additional elements and degrees of freedom (dof) with an increase in size [5][6][7][8][9][10]. Indeed, they are also attractive because they can be built using a standard patch. Hence it can have the same form factor as typical GNSS antennas. Some commercial off the shelf (COTS) patch antennas are even built with both feeds [4] and the Stanford DPA is built using such an antenna. Based on Figure 2, Equation 1 defines the inputs and outputs to the hybrid coupler as a vector, y , representing the RHCP output, X axis input, Y axis input and LHCP output, respectively. Given this definition, the action of the ideal hybrid coupler is given by matrix A shown in Equation 2 [11].

$$y = [RHCP_{out} \quad X_{in} \quad Y_{in} \quad LHCP_{out}] \quad (1)$$

$$A = \begin{bmatrix} 0 & j & 1 & 0 \\ j & 0 & 0 & 1 \\ 1 & 0 & 0 & j \\ 0 & 1 & j & 0 \end{bmatrix} \quad (2)$$

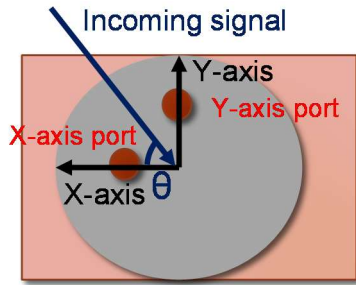


Figure 1. Configuration of DPA antenna elements

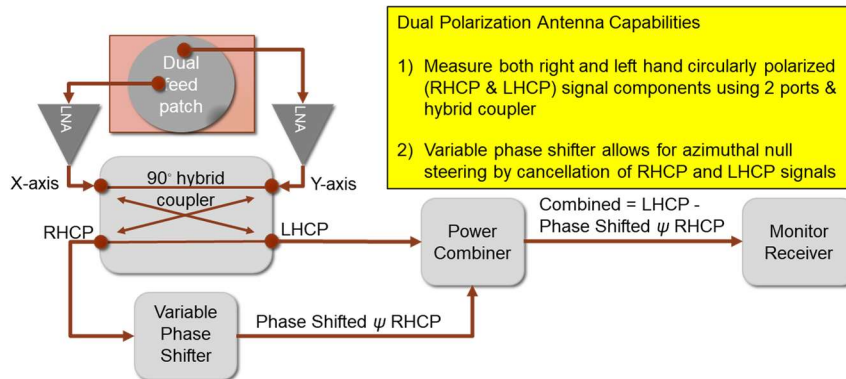


Figure 2. Initial Architecture Design of Stanford DPA

The Stanford dual polarization antenna further realized the potential benefits of GNSS DPA by showing that it can also determine direction of arrival which can aid in spoof detection and also provide static heading [3][11]. Analysis indicated and experimental test demonstrated that our DPA can determine relative DOA as well as rough elevation angle [1] [2]. The design, which follows the architecture shown in Figure 2, was prototyped and field tested under interference conditions [11]. It uses a hybrid coupler to generate RHCP and LHCP from the signal received in the x and y ports of the antenna. For our initial implementation, DOA determination is conducted first by systematically shifting the RHCP signal using a variable phase shifter controlled by a microcontroller. The phase shifted RHCP signal is combined the LHCP signal to be processed by a monitor receiver whose outputs are used to determine DOA. The details of DOA determination are discussed in the next section. While our initial implementation (so called hybrid) was built using large modular components, the architecture was such these components could be replaced by small surface mount discrete components. The architecture also supported the use of standard GNSS receiver such as the COTS IC used in smartphones and automotive applications. It simplifies signal processing into analog combinations for traditional processing by a COTS receiver. The overall surface mount technology (SMT) design was first prototyped using evaluation boards for each components. Once validated, a printed circuit board (PCB) version (version 1 PCB DPA), shown in Figure 3, was produced [1].



Figure 3. Stanford Printed Circuit Board (PCB) Dual Polarization Antenna Version 1 [1]

Direction of Arrival using DPA

Direction of arrival can be determined by the DPA provided that the signal of interest traverses the antenna ground plane before entering the antenna. Boundary conditions result in the signal becoming linearly polarized when traversing the ground plane, regardless of initial polarization. This condition will occur if the antenna is on a reasonable ground plane (~0.3 m radius is adequate) and the incoming signal is not coming from too high an elevation above the receiver. The idea is shown Figure 4. The linearly polarized signal can be decomposed into RHCP and LHCP components which have a phase difference, ψ , that is related to the incoming DOA, θ . If we assume that θ is the offset angle of the incoming signal from the x-axis of the antenna, then we can define an incoming signal to the antenna by Equation 3 using incoming angle shown in Figure 1. Equation 4 shows the result after going through the hybrid coupler. The result is divided into RHCP and LHCP components. If we express the output in exponential form, we can clearly show that the phase difference between RHCP and LHCP (ψ) is given by Equation 5. Hence, if we find the true phase offset between the RHCP and LHCP, then the DOA relative to the x-axis can be found. As seen in the equation, the DOA estimate has a 180 degree (π radian) ambiguity – the same measured phase offset will be found for a signal coming with an incoming angle of θ or $\theta + 180^\circ$. Noise and other signals (e.g. direct RHCP signals) will result in phase offset and hence DOA errors.

$$y = [RHCP_{out} \quad Xin \quad Yin \quad LHCP_{out}] = [0 \quad \cos\theta \quad \sin\theta \quad 0] \quad (3)$$

$$Ay = [\sin\theta + j\cos\theta \quad 0 \quad 0 \quad \cos\theta + j\sin\theta] = [e^{j(\pi/2-\theta)} \quad 0 \quad 0 \quad e^{j(\theta)}] \quad (4)$$

$$RHCP_{out} = e^{j(\pi/2-\theta)}; LHCP_{out} = e^{j(\theta)}; \psi = \frac{\pi}{2} - 2\theta \quad (5)$$

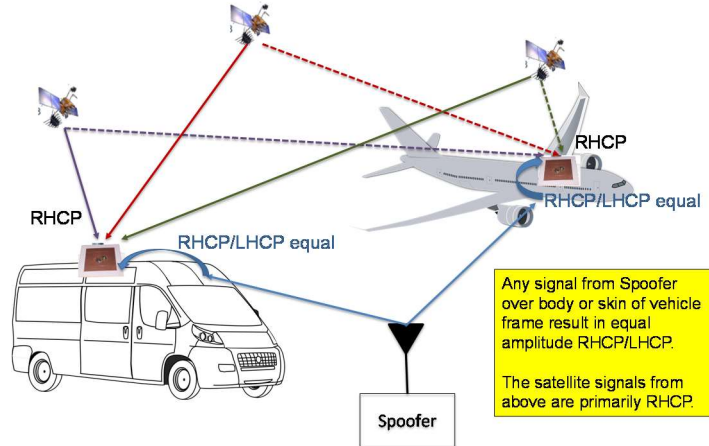


Figure 4. Dual Polarization Antenna Concept for Spoof Determination

While the RHCP and LHCP signals will have the relationship defined in Equation (5), how does one process the signal to find the phase difference? One way is to apply different phase offsets to one of the signals and determine when the RHCP and LHCP align (in phase) or anti-align (180 degrees out of phase). In other words, apply phase offsets to see which one results in the peak or trough (null) of the combined RHCP and LHCP signal. The desired phase offset yields ψ . In our COTS GNSS implementation, we choose to offset the RHCP signal and look for the null. A more direct way is to track both RHCP and LHCP signals and calculate their respective phases at each instant in time to get the phase difference. This approach generally requires a more flexible receiver such as an SDR or a specially designed IC.

The first concept was implemented using a COTS GNSS receiver and the standard outputs of the receiver. Essentially, a phase shift was selected by the microcontroller and applied to the RHCP signal, this was subtracted from the LHCP signal and then fed to the COTS receiver which provided the carrier to noise ratio (C/No) of the resultant combination. The microcontroller steps through all phase shifts sequentially. Results with genuine GPS satellites shows the variation of C/No for this process in Figure 5 [1]. Phase difference and thus DOA (relative to the antenna x axis) is then derived from the phase offset resulting in the null as shown in Equation (5). Importantly, the test shown in the figure demonstrates that even with a RHCP signal (i.e. the genuine GPS signal), there will be significant linearly polarized component at elevation angles below 60 degrees. Hence, there are many scenarios that a DPA may provide useful DOA measurements for spoof detection.

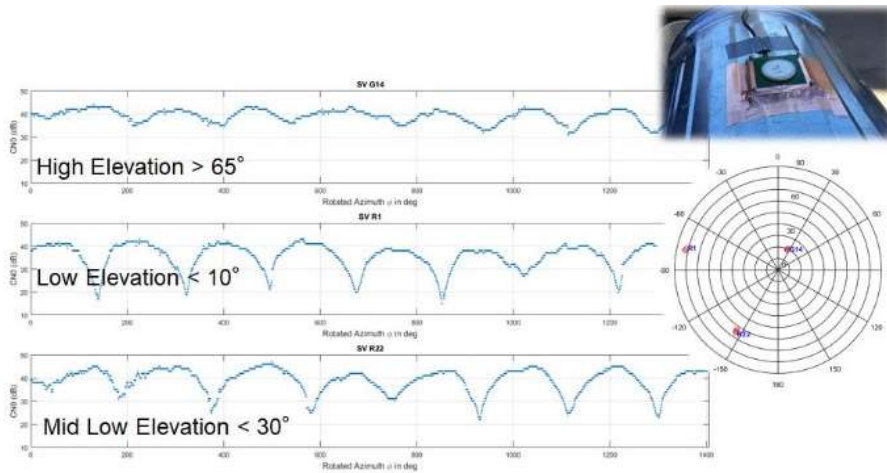


Figure 5. C/N_0 vs. Rotation of LHCP component for different satellites: high (top), low (bottom), very low (middle). At low and very low elevation, rotation of LHCP component to the correct angle can significantly cancel out RHCP, ~ 180 second to complete all rotations [1]

The limitations of the sequential process can also be seen in the figure. In this test, it took about 192 seconds (3.2 minutes) to complete on full cycle of phase shifts. The microcontroller in the Stanford DPA is used to adjust the amount of dwell time on each phase shifted combined signal. However, there is a limit as it takes time for the receiver to process each signal. Furthermore, the receiver averages the C/N_0 over a moving window which means our current measurement is affected by results from prior phase shifts. Hence longer dwells reduce the influence of past phase shifts and provide higher fidelity measurements. Version 1 used cycle periods from 51.2 to 256 seconds to produce useful DOAs. Shorter scan periods led to noisy, unreliable measurements. This paper will discussed improvements in the circuit design and coding to reduce cycle periods need to produce useful DOA to as low as 2 seconds.

FASTER DIRECTION OF ARRIVAL DETERMINATION TIMES

For a system practical for application such as flight, the DPA DOA determination must be sped up. We examined ways to have fast DOA determination with the two approaches previously discussed.



Figure 6. Version 2 of Stanford Printed Circuit Board DPA with COTS GNSS and RHCP/LHCP out mounted on aluminum ground plate

First, we examined our past version 1 PCB DPA design to develop means of decreasing the scan period needed for effective DOA determination. The version 1 PCB DPA, which uses a COTS GNSS, was used in tests in 2017 and 2018 [1][2] and could step through a full cycle of phase offsets in about 2 seconds. However, the noisiness of the measurement and our estimates of the phase offsets made the practical scan period much higher – on the order of 50 seconds or more. Lower scan periods would lead to noisy measurements that resulted in poor and generally unusable DOA estimates. Hence, we made several improvements to the design. To decrease measurement noise and error, we used a different hybrid coupler and integrated the GNSS IC directly onto the PCB with a microstrip instead of a wire used in version 1. The former provides cleaner measurements while the latter allows for better alignment of phase step with the GNSS output. We also changed the processing pipeline to place the low noise amplifier (LNA) after the hybrid coupler so that any differential phase offsets from the LNA does not get remixed by the hybrid coupler. Additionally a faster microcontroller was used in the new design to record the phase shift value from the variable phase shifter. The prior version inferred differences based on the shift size and rate. The new version, version 2 DPA PCB, is shown in Figure 6. Additionally, this version was built to provide both raw RHCP and LHCP signals through two SMA feeds as well as processing through the on-PCB COTS GNSS IC, though not simultaneously due to design limitations. The architectural design using COTS GNSS IC is shown in Figure 7 while the SMA feeds, placed after the LNAs, are used to provide RHCP and LHCP outputs to digitize for use with an SDR.

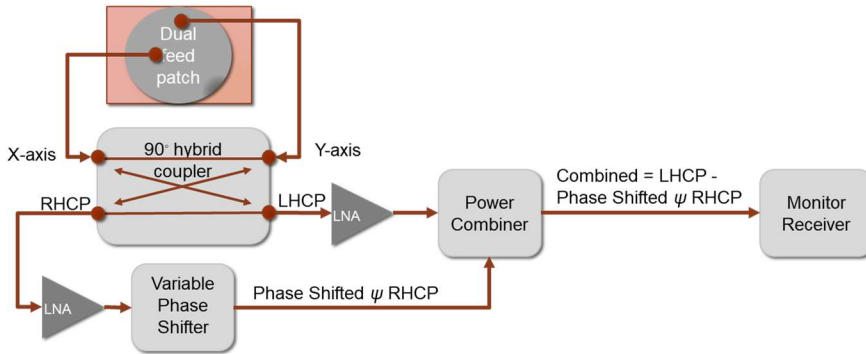


Figure 7. Architectural Design of Version 2 PCB DPA (COTS GNSS IC processing chain; SDR uses digitized signals from SMA feeds connected to each LNA)

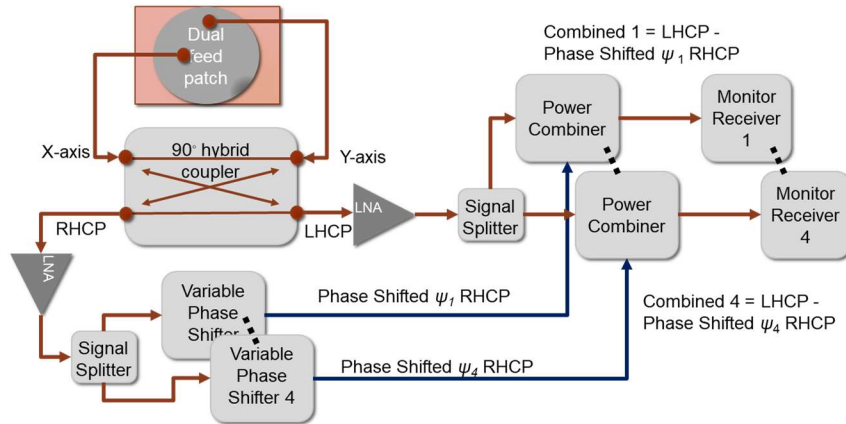


Figure 8. Parallelized processing for dual polarization antenna direction of arrival determination using commercial GNSS receivers as monitor receivers

The revised version of the PCB DPA was tested using various scan periods to verify improved performance. As seen later, using step sizes of 11 degrees, on air tests showed useful DOA performance at scan periods as low as 2 seconds. The DOA accuracy did not degrade much when compared to higher periods such as 4 seconds. The performance is comparable to version 1 at its much higher cycle period. Lower rates are possible with some noticeable reduction in fidelity. With the new design, the output rate of the GNSS IC starts to become a limitation. Hence, lower rates are still possible with this architecture with higher output rate GNSS ICs. Additionally, DOA processing using COTS hardware can be further

expedited as discussed in our previous paper [2] through parallel processing. As shown in Figure 8, the concept is to use many COTS receivers, as they are relatively inexpensive, to parallel process multiple phase shifted combinations at the same time. With the notional design using four COTS GNSS IC shown in Figure 8, the DOA determination is speed up by a factor of four meaning that we can have our COTS design support 2 Hz DOA updates.

If more flexible processing is available, faster and more powerful techniques can be used on the RHCP and LHCP signals. One benefit of software processing is that we can process the phase difference at each time step allowing for angle determination at every epoch. This helps limit means to circumvent the detection. It also provides many DOA determinations that can be averaged over a few seconds which may provide some improvements DOA estimates. Finally, it also allows for implementation of interference mitigation. We examine these important benefits (interference mitigation, heading estimate in nominal conditions) through field experiments conducted using our Stanford DPA. The tradeoff here is that this approach requires more powerful and flexible processing that mandates use of a dedicated bespoke receiver rather than one or many low cost, low power COTS IC receivers.

The SDR based DPA digitalizes the RHCP and LHCP signals from the hybrid coupler for processing by the SDR. Thus the same antenna, front end and hybrid coupler is used for either SDR or COTS IC GNSS processing. The output for each polarization goes to SMA connectors which are connected to a universal software radio peripheral (USRP) X300 to capture and digitize the signal. The USRP daughter cards serves as the analog to digital converter (ADC). These cards are frequency synchronized and digitizes in phase and quadrature data at the same time. But they are not phase synchronized so there is a phase offset between the two data streams. The data is recorded onto hard drives and replayed into a modified version of our software receiver developed to support this DOA determination. The SDR is based on our real-time CRPA receiver [12].

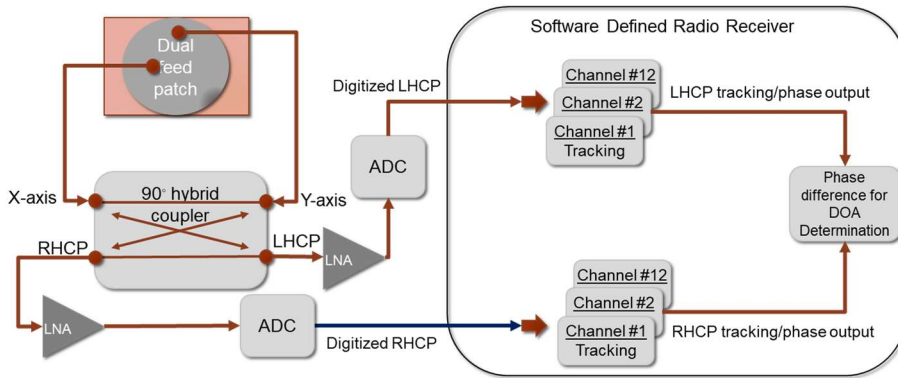


Figure 9. Post tracking processing for dual polarization antenna direction of arrival determination using a software defined radio receiver

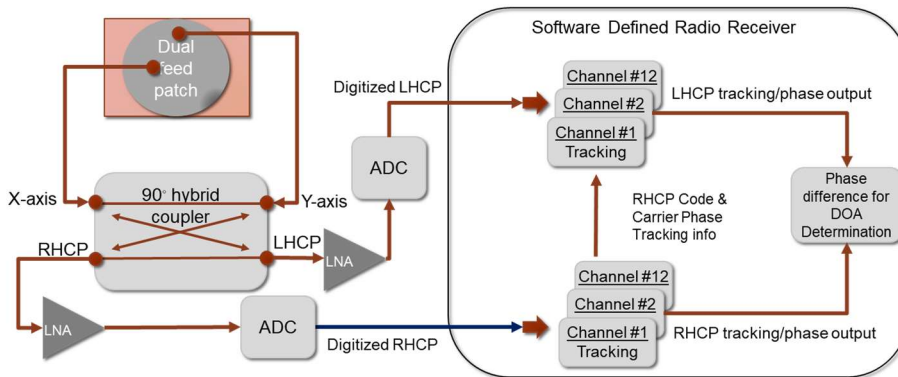


Figure 10. Post tracking processing for dual polarization antenna direction of arrival determination using a software defined radio receiver with LHCP tracking aided by RHCP tracking

Several means of processing are considered. An efficient way is to have two channels for each satellite, one each for the tracking the RHCP and LHCP component of the signal, respectively, as shown in Figure 9. The phase offset is calculated by

looking at the difference in phase lock loop (PLL) measurement for the RHCP and LHCP signal at the same instant in time. Hence the tracking needs to be synchronized to the same clock. The tracking can otherwise be done independently. This approach is also attractive as it may lend itself to implementation with COTS GNSS receivers, provided that we are able to have them utilize a common clock so that we can make sample by sample phase comparisons. One challenge is that the Stanford SDR is not a high sensitivity receiver and requires about 35 dB-Hz for tracking which is more difficult to achieve for the typically weaker LHCP signal. Experience has shown that the RHCP component tends to be much stronger and so our architecture leverages the tracking loops in the RHCP for processing the LHCP signal. RHCP code phase and carrier frequency are used to process the LHCP signal yielding the in phase and quadrature LHCP output. This allows us to calculate the LHCP phase even at LHCP signal levels below our receiver tracking threshold thus enhancing our ability to perform the DOA determination. Hence, the LHCP tracking channel is neither closed loop nor independent of the RHCP tracking. The design is shown in Figure 10. A similar aiding is also done by the Septentrio receiver in used for DPA research as part of the Field Aware Navigation and Timing Authentication Sensor for Timing Infrastructure and Centimeter level positioning (FANTASTIC) project [13]. Since we have a SDR, we can perform both the RHCP aided and unaided versions of LHCP signal processing. The result is that from the software receiver, we get the phase and carrier to noise ratio (C/No) for the unaided tracking loops (RHCP and LHCP) of each satellite but only phase outputs for the aided LHCP. The latter is because we do not track but simply utilize RHCP phase tracking information (code phase, frequency) to get LHCP in phase and quadrature components. With just the phase output, which should be better than the unaided LHCP phase output due to the stronger RHCP signal, we do not have a clear sense of the quality of the calculated LHCP phase. We will examine this in the results.

Additionally, with the SDR, we can form one more combination that can be used to mitigate and determine the direction of an interference signal. We can form a combined signal, sig , that is the combination of the LHCP signal and a phase shifted RHCP signal. We choose the phase shift to minimize the power of sig which effectively forms a null in the direction of most incoming power (presumably the interference source). This is presented in Equation (6). The phase shift calculated provides an indication of the direction of the interference source.

$$\min_{\phi} |sig(\phi)|, sig(\phi) = LHCP_{out} + e^{j(\phi)} * RHCP_{out} \quad (6)$$

EXPERIMENTAL SET UP & FIELD EXPERIMENTS

We tested the new version of the PCB DPA in the field to validate its improved operational capabilities and to demonstrate the utility of DPA for flight applications. Static tests of several revisions of the version 2 PCB indicated that the design was capable of achieving the desired fast performance. We partnered with the US Air Force Test Pilot School (USAF TPS) at Edwards Air Force Base (AFB) to fly our prototypes of the DPA. Ground and flight tests were conducted in September 2019 at Edwards AFB. For the testing, the PCB DPA was mounted on the top of a C-12J (Military version of the Beechcraft 1900) operated by the 586th Flight Test Squadron, Holloman AFB, NM. To support flight tests, a custom 1 foot diameter aluminum plate was built to mount the antenna onto the aircraft. The plate also provided a ground plane for the DPA. A 3-D printed housing covered the antenna and the unit was completely sealed using adhesives to survive the airborne environment. Air worthiness tests were performed on the antenna and mounting, shown on the aircraft in Figure 11, to ensure that it could safely operate within the C-12J flight envelope.



Figure 11. Version 2 Stanford DPA mounted on C-12J (left); Flight rack of data collection equipment for C-12J including USRP X310 and data collection computer (right)

For the flight test, we operated the DPA and a survey grade receiver connected to a separate antenna. For the DPA, we either collected raw intermediate frequency (IF) data from the RHCP and LHCP feeds (i.e. DPA in SDR mode) or processed data from the COTS IC GNSS but not concurrently. So we cannot directly compare the two techniques in simultaneous performance. Even if possible, this would not be a fair comparison as the COTS receiver is far more sensitive than our software receiver. The IF data was collected at 2 mega samples per second (Msps) at 16 bits for both the in phase and quadrature channels. Processing of this data by software receiver was done after the flight. In COTS GNSS mode, the DPA was configured for the flight test to complete a full 360 degree scan every 1.9636 seconds. This was done using phase offset steps of 11 degrees which was adequate to accurately find the phase difference of the null. Each phase offset was used for a 60 millisecond (ms) interval to give the COTS GNSS receiver time to measure its effects. This step rate resulted in a scan period of 1.9636 seconds. The survey receiver was used to provide a truth reference for position and heading. The true heading was estimated using by differencing GNSS position estimates which yields the direction of travel, commonly known as course over ground (COG). While COG does differ from true heading due to cross wind effects, this difference is not significant for our evaluation given our other errors.

The testing was conducted in non-spoofing and predominately nominal conditions. The flight test consisted of 8 flights with two experiencing planned GNSS interference. These flights were conducted as part of the overall DT Navfest GPS jamming exercise hosted by Edwards AFB. Some of flight scenarios conducted and shown in this paper includes: 1) straight level flights, climbs, descents, 2) spiral climbs, descents, 3) dynamic maneuvering (including 60 degree, 2-g turns). The more extreme scenarios were designed to test the DPA in conditions that could affect its performance. For example, high bank turns significantly effects DPA measurements as well as making its DOA measurements no longer planar to the azimuthal direction. Hence, heading estimates in this condition would be considered suspect as a basic assumption of the calculation (measurements are in the azimuthal plane) are violated.

TEST RESULTS

The key goals of the test were to verify the efficacy of the DPA measurement and demonstrate its capability for rapid DOA determination for spoof detection in flight. We also wanted to examine the other benefits of DPA. We can check measurement consistency of each satellite DOA. Ideally, they should vary together as most of the change in DOA in flight is due to heading, a common source for all DOAs. With some knowledge of true heading and position, we can test performance and efficacy by examining the DOA accuracy, variability and availability. We also examined heading determination under nominal conditions as this is a useful side benefit of the DPA.

We evaluated measurement consistency by checking, for each satellite i , that its determined DOA (θ_i) are consistent with its known satellite azimuth direction (azi_i). By satellite azimuth, we mean the satellite direction relative to true north rather than the orientation of the antenna. These definitions are shown in Figure 12. There are several ways to examine measurement consistency. For the paper, we check by essentially calculating the heading, the direction of the aircraft relative to true north. Assuming that the x-axis of antenna is aligned with the body of the aircraft, Equation (7) and Figure 12 shows that the DOA (θ_i), angle between the x-axis of the antenna and the incoming satellite signal, plus the offset of that axis from the aircraft body centerline (a) plus the heading (hdg) equals the satellite azimuth relative to true north (azi_i). If we take this equation and combine it with the derived phase difference measurement equation for our DPA, i.e. Equation (5), we get Equation (8). If the alignment of our antenna relative to the aircraft body, a , we can lump this constant offset with the 45 degree ($\pi/4$) phase term into a constant, $c = \pi/4 + a$, as these two are constants that should be the same for all satellites. This is shown in Equation (9) which we can rearrange to get estimated heading derived from the phase difference measurement from satellite i given in Equation (10). Ideally, the estimated heading should be the same for each satellite, subject to a 180 degree ambiguity. So we can check consistency between measurements in several ways by making the calculation on the right side of Equation (9) or (10) for each satellite phase difference over time. We can check if these measurements are consistent with each other (e.g. their difference accurately reflects satellite azimuth difference) and if they are consistent with heading if true heading or a proxy (e.g. COG) for it is known. In this paper, we use COG.

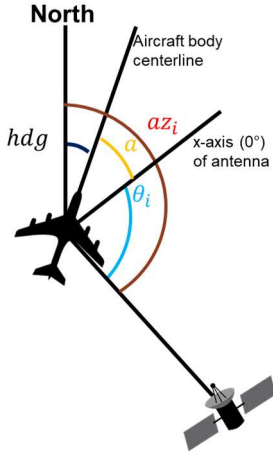


Figure 12. Relationship between satellite azimuth (azi), direction of arrival (θ_i) and aircraft heading (hdg)

$$azi_i = \theta_i + hdg + a \quad (7)$$

$$hdg = azi_i - \frac{\pi}{4} + \frac{1}{2}\psi_i + a \quad (8)$$

$$hdg + \left(\frac{\pi}{4} - a\right) = hdg + c = azi_i + \frac{1}{2}\psi_i \quad (9)$$

$$\widehat{hdg}_i = azi_i + \frac{1}{2}\psi_i - \left(\frac{\pi}{4} - a\right) \quad (10)$$

We can also calculate the statistical mean and variance of the DOA measurements. If we have true heading, we can calculate the error of the heading as derived from each DOA. We can use Equation (10), provided we can estimate the fixed offset, a , and assuming that the satellite azimuth is known. One way to calculate a is to find the value from initial ground tests either statically with the aircraft point in a known direction or the aircraft traveling in a straight known course. Once the offset is derived, this should stay fixed as long as the antenna is not moved. With DOA derived and true headings, we can derive an error estimate and hence the statistics on DOA error in different parts of the aircraft test profile.

Direction of Arrival Performance of DPA COTS GNSS

We first examine the DOA determination of the DPA using the COTS GNSS. Flight data from September 18 2019 is used to illustrate the performance. Figure 13 shows an example of DOA determination over a roughly 20 minute (1200 second) period at the start of the mission. During this time, the aircraft was on the ground and static. It demonstrates the capability of the implementation to get 0.5 Hz DOA from many satellites including GPS (G), Galileo (E), GLONASS (R) and SBAS (S). The results show that while many satellites have low variation DOA determination and that the DOA estimate was reasonably stable in most cases.

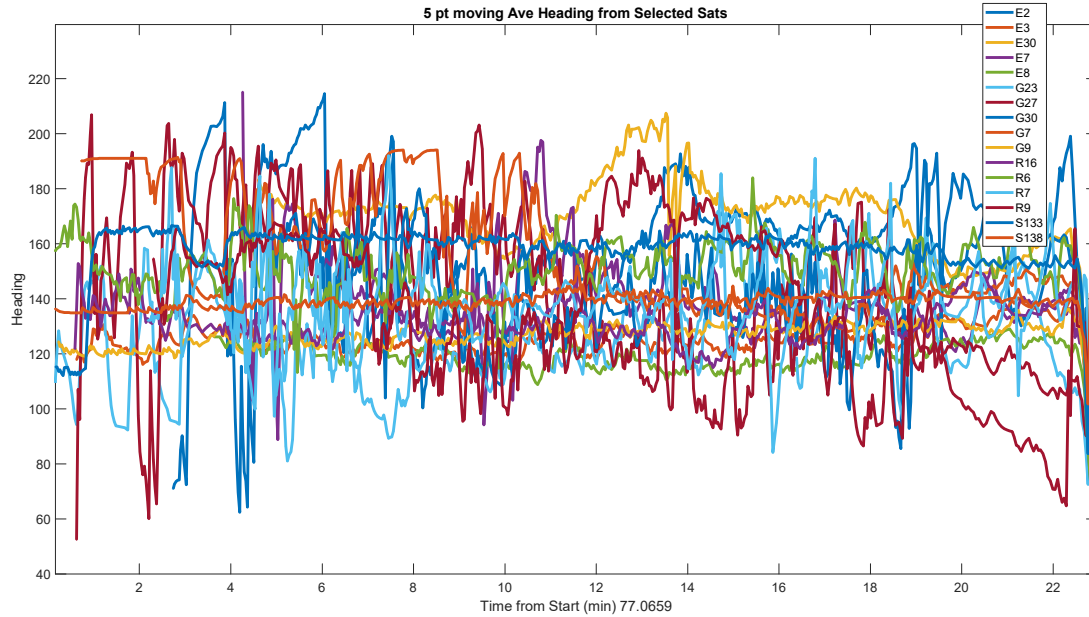


Figure 13. Individual Heading Estimate derived from COTS DPA DOA (2019-09-18) with 5 point moving average; starting 22.0659 (10:04 PM)

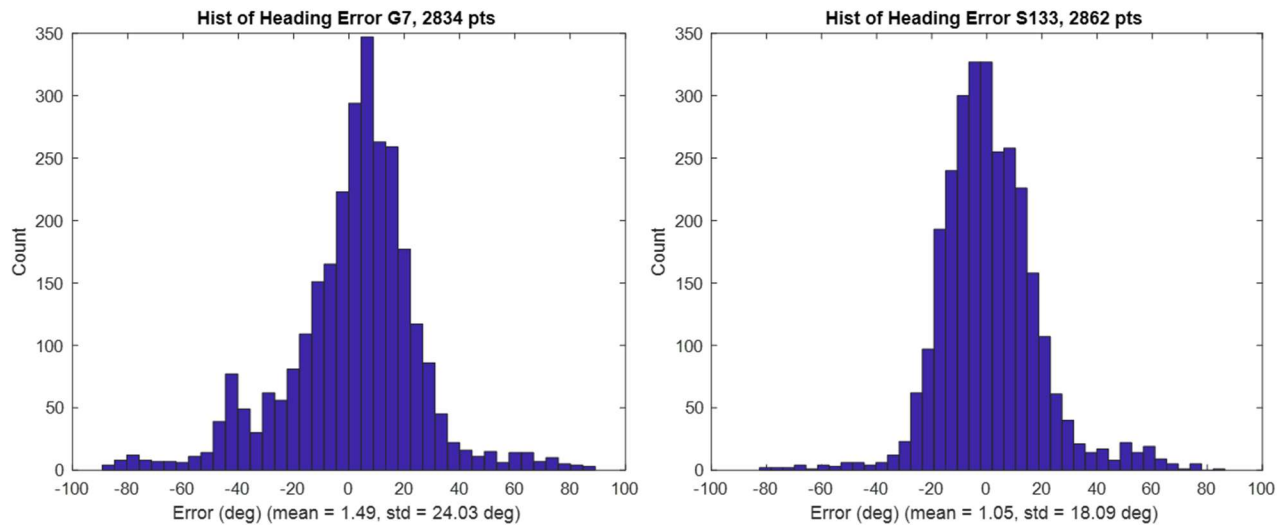


Figure 14. Direction of Arrival Error Estimates from COTS DPA from ~ 2 hour flight (2019-09-18)

Figure 14 shows the histogram of the DOA error of two satellites over the course of the nearly two hour flight on September 18th. The error is calculated by taking the difference of the Kalman filter estimate of heading, shown previously, using all satellite DOAs from that derived from each individual satellite DOA. COG calculated from GNSS is not used as it uses a fixed reception pattern antenna (FRPA) and cannot generate a valid answer when static or at low velocity. These satellites used in the figure were visible much of the flight. Examining all satellites, the typical statistics generally show some bias, usually less than 10 degrees and standard deviation between 18 to 30 degrees. This is similar to what has been seen previously [14].

From these DOAs, estimated headings from individual satellite measurements are determined. Several methods of determining heading with the DPA is possible and described in [3]. Figure 15 shows heading derived using least squared solution weighted by the estimated error variance of each measurement. This is then fed to a Kalman filter which helps with

the 180 degree ambiguity resolution for each DOA. The error variance is estimated based on several factors in the measurement such as the depth of the C/No drop (null depth) and the general pattern of the null search [3][14]. Additionally, compensation is made in the calculation for banking as this affects the quality of the DOA measurement. To compare, COG derived from GNSS position, velocity, time (PVT) is also plotted. The derived heading error is relatively low with all standard deviation of 7.3 degrees for all valid COG over 2 m/s. If we limit the bank angle to 30 degrees, then the standard deviation of error is 5.7 degrees. Again, static or low velocity periods are excluded as COG is not accurate at these times.

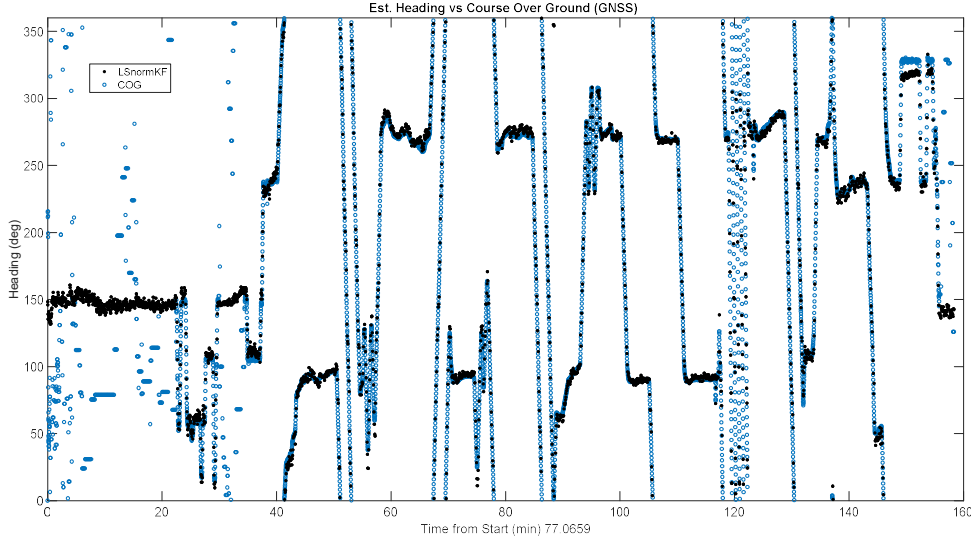


Figure 15. COTS DPA derived heading and GNSS derived Course over Ground (COG) for 2019-09-18; starting 22.0659 (10:04 PM)

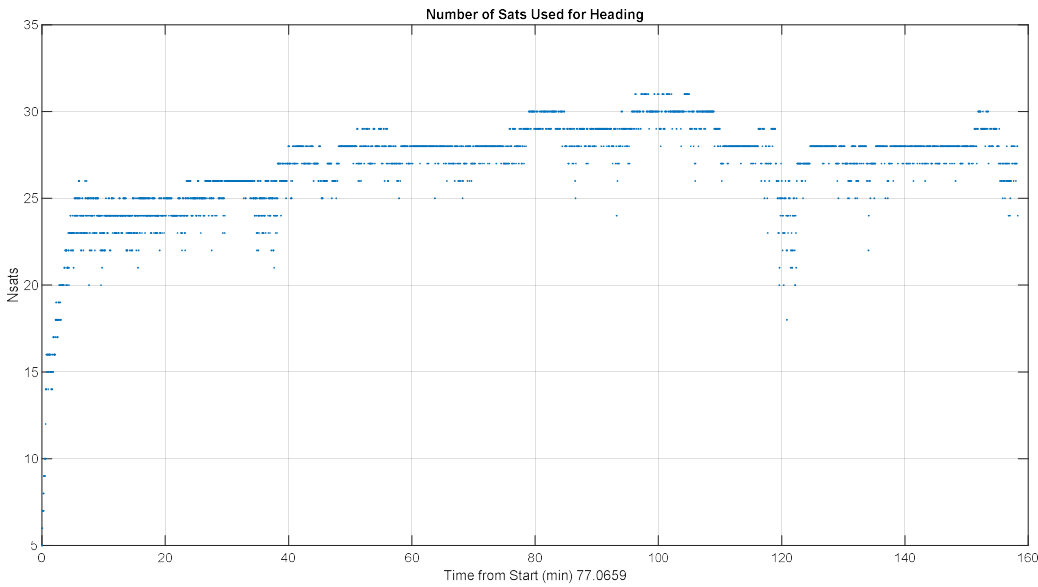


Figure 16. Number of satellites from COTS ASIC DPA used for heading estimate (2019-09-18); starting 22.0659 (10:04 PM)

Given the relatively large, though expected, DOA error variance from the COTS DPA, is relatively low. Several factors contribute to the low errors. First is the high number of satellite measurements available. Figure 16 shows the number of satellites used for the heading calculation over the course of the mission. With three GNSS and SBAS available, we had generally over 25 satellites with DOA measurements with this number occasionally exceeding 30. Second, airplanes are typically low multipath environments. Multipath can significantly affect the DOA estimate, depending on where it is coming from and how strong it is. It can cause measurement biases that may not easily average out. Fortunately, the benign multipath environment makes this error not a significant concern.

Direction of Arrival Performance of DPA SDR GNSS

The performance of the DPA in SDR mode was examined in a similar manner. The SDR processed RHCP and LHCP phase values which are then differenced to get the DOA. Both 20 ms and 100 ms integration periods were used with 100 ms having better performance and less outliers. The paper shows results using 100 ms integration period. Unless otherwise stated, the results use the aided LHCP phases. As mentioned previously, USRP digitized using two daughterboards which are frequency but not phase synchronized. Hence we have to modify Equation (7) to add a phase bias that changes each time the USRP is started. This yields Equation (11). Taking Equation (10) and (11), we get Equation (12) giving us the estimated heading. The constants, all lumped into d , is calculated on a per data collection basis.

$$\psi = \frac{\pi}{2} - 2\theta + b_{usrp} \quad (11)$$

$$\widehat{hdg}_i = az_i + \frac{1}{2}\psi_i - \left(\frac{\pi}{4} - a\right) - \frac{b_{usrp}}{2} = az_i + \frac{1}{2}\psi_i - d \quad (12)$$

We start by first examining the consistency of the estimated heading from each individual DOA from the SDR. Each DOA measurement is processed with its satellite azimuth to get heading after estimating the constant from the full data set using all available satellites. So like in the COTS GNSS section before, we can see the consistency of the measurements from each satellite. Figure 17 and Figure 19 shows the results for a ground test on September 9 and a flight test on September 10, respectively. Figure 18 shows the ground track September 9th data over time – these times correspond with the second x-axis time labels in Figure 17. Figure 17 shows that on the static periods from 0 to 250 seconds and 290 to 310 seconds, the calculated headings (plus offset) are consistent between the satellites shown in the figure. As mentioned previously, the DPA has a 180 degree ambiguity. For the figures, we fix the 180 degree ambiguity by chooses the value that best matches the COG. Periods of motion have greater inconsistencies, especially from 310 to 460 seconds, between satellites reflecting a greater spread of errors. The statistics of the error for all are shown in Table 1. It shows comparatively small biases (< 10 degrees) with the exception of PRN 12 and standard deviations of 11 to 37 degrees. Looking at the plot, we can see these variations occur at fine level indicating that averaging over a short period (~ 1 second) can reduce error.

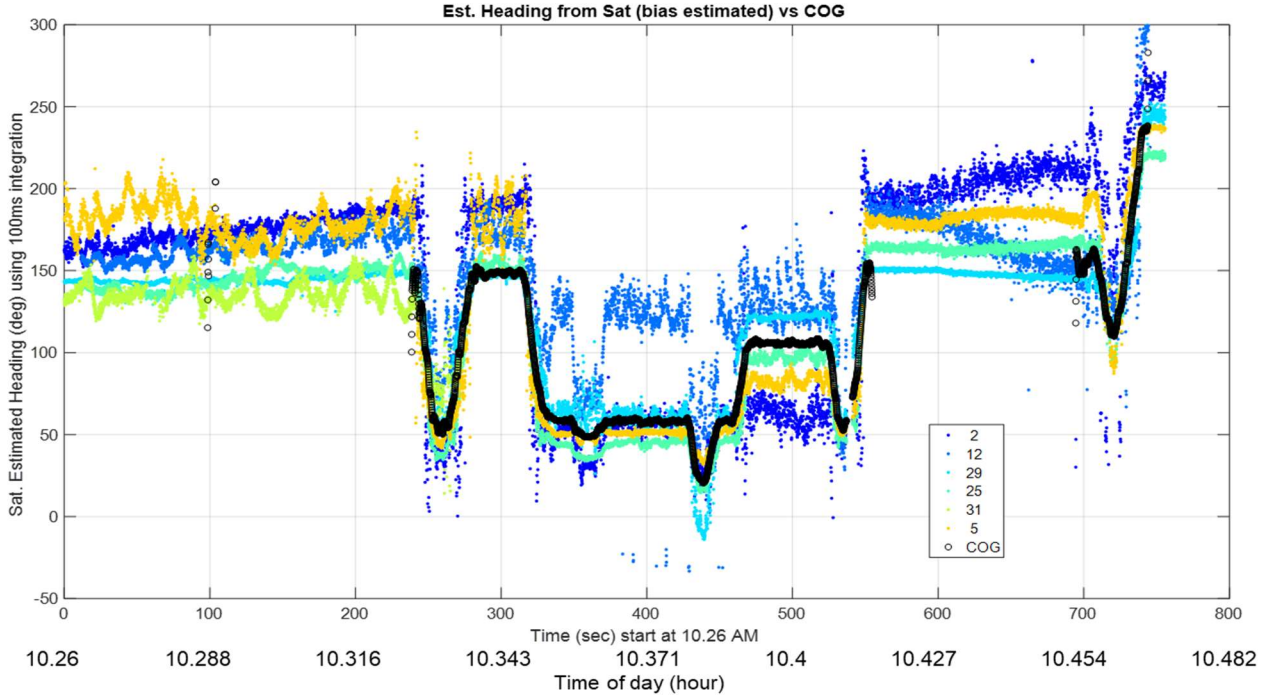


Figure 17. Estimated Heading Corrected with Estimated Bias ($d = 46^\circ$) and 180° ambiguity for each tracked GPS satellite on 2019-09-09; starting 10.26 (10:16 AM)



Figure 18. The aircraft taxi path for 2019-09-09 showing several generally constant direction segments

Table 1. Mean and Standard Deviation (std) of GPS Satellite DOA (in degrees) calculated heading relative to COG (assuming COG is true heading) for segment shown in Figure 19. PRN 12 not used for mean calculation (September 9 2019)

| Sat PRN (GPS) | 2 | 12 | 29 | 25 | 31 | 5 |
|---------------|------|------|------|------|------|------|
| Mean (deg) | 3.1 | 33.2 | 4.3 | -8.4 | 1.8 | -0.9 |
| Std (deg) | 36.6 | 2.1 | 13.4 | 10.7 | 19.0 | 21.8 |

Figure 19 presents a set of headings calculated from individual satellite measurements as well as the COG calculated from GNSS PVT from two hour flight on September 10. Again, a bias offset, which differs from that of September 9 is calculated using all satellites in view. The headings generally follow the movement of the calculated COG which suggests that phase difference measurements do correspond with DOA. The histogram of heading errors of two example satellites relative to COG during this flight is shown in Figure 20 which shows performance similar to that of the COTS GNSS. However, the distribution is less Gaussian and some have multi-modal behavior. Table 2 shows the mean and standard deviation of the error for all used satellites for periods where we have COG. The mean and standard deviations are generally larger than that seen in the prior (ground only) results.

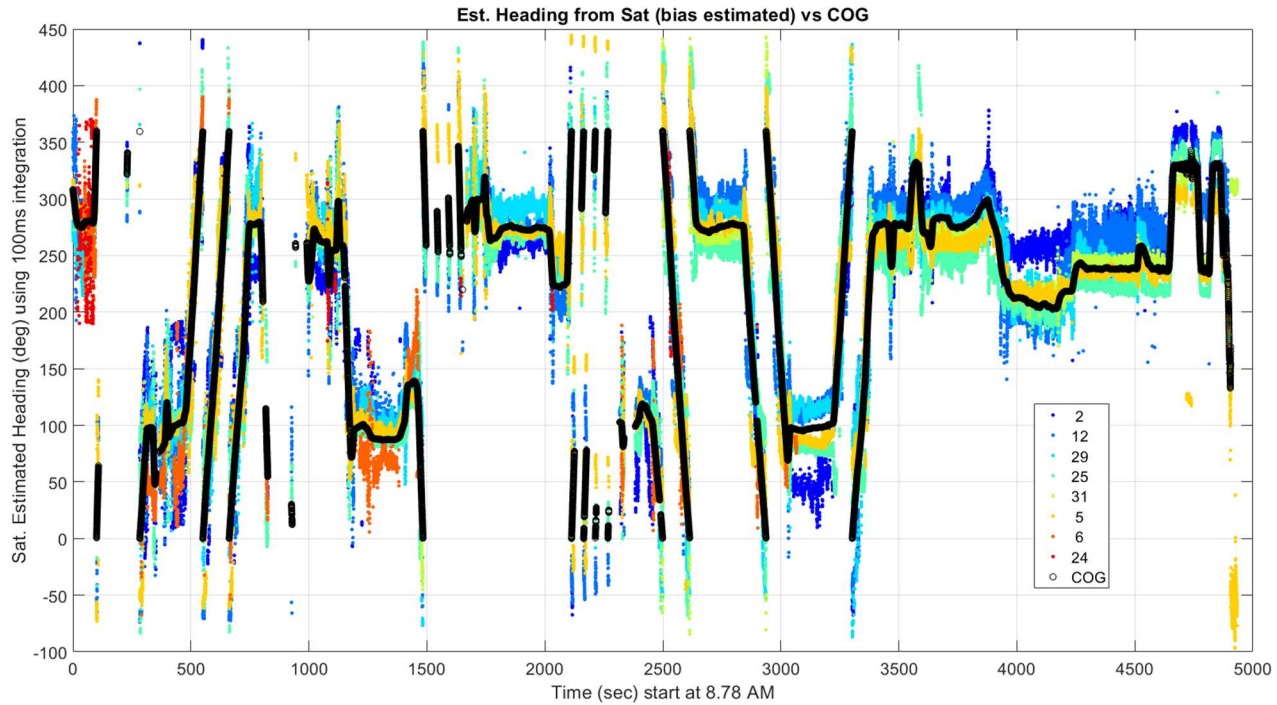


Figure 19. Estimated Heading Corrected with Estimated Bias ($d = 7^\circ$) and 180° ambiguity for each tracked GPS satellite for flight segment on 2019-09-10; starting 8.78 (8:47 AM)

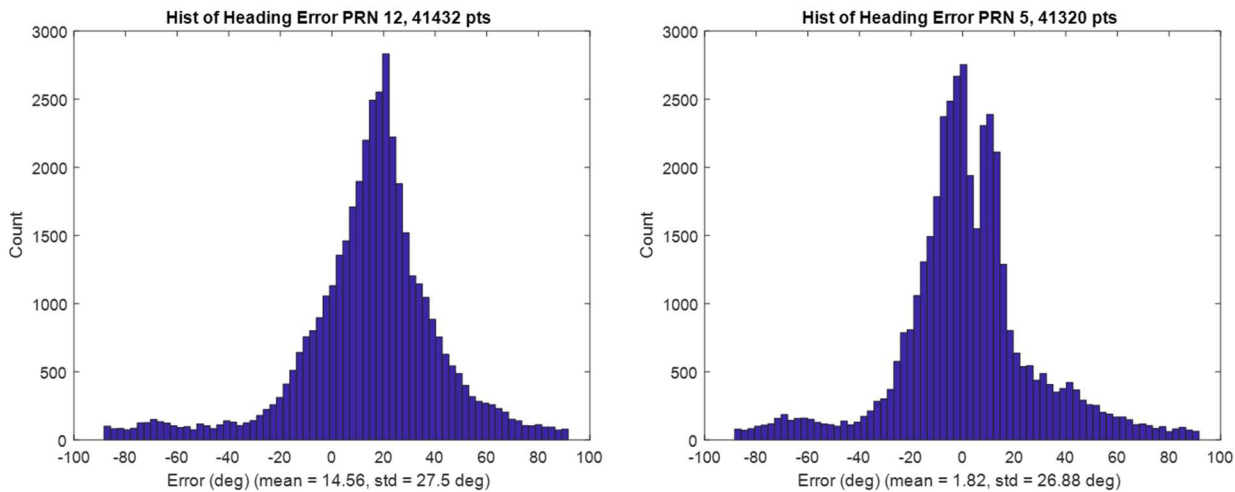


Figure 20. Direction of Arrival Error Estimates with SDR approach using RHCP aided LHCP phases from 2 hour flight (2019-09-10)

Table 2. Mean and Standard Deviation (std) of GPS Satellite DOA (in degrees) calculated heading relative to COG (assuming COG is true heading) for segment shown in Figure 19. PRN 12 not used for mean calculation (2019-09-10)

| Sat PRN (GPS) | 2 | 12 | 29 | 25 | 31 | 5 | 6 | 24 |
|---------------|------|------|------|------|------|------|------|-------|
| Mean (deg) | 13.0 | 14.6 | 5.7 | -5.1 | -3.2 | 1.8 | -0.9 | -12.1 |
| Std (deg) | 34.7 | 27.5 | 22.0 | 27.8 | 12.6 | 26.9 | 30.1 | 42.6 |

Next we examined the calculated heading using all the satellites. In this case, we have far fewer satellites than when using the COTS receiver for several reasons. First, our SDR has lower sensitivity. Second, we do not have GLONASS since those frequencies are not capture and Galileo as our software receiver does not process the signal. Figure 21 and Figure 23 show the heading estimate using all available satellites DOA for the September 10 flight and September 9 ground segment, respectively. No Kalman Filter is used and the best value for the 180 degree ambiguity is used. Figure 23 shows that heading

for the path shown in Figure 18 is reasonably matched with worst case being two straight segments where the DOA heading is either too high or too low by about 20 degrees. Figure 21 shows the entire flight on September 10 and it generally shows good heading to COG match, especially on the straight segments. The overall heading differs generally less than 10 degrees from COG. However, the match is not as good in the turn segments, where the COG rapidly cycles from 0 to 180. This is not surprising as these are high bank turns which violates the assumptions we have for using the DPA to calculate azimuthal plane DOAs. The DOAs calculated are no longer in the azimuthal plane.

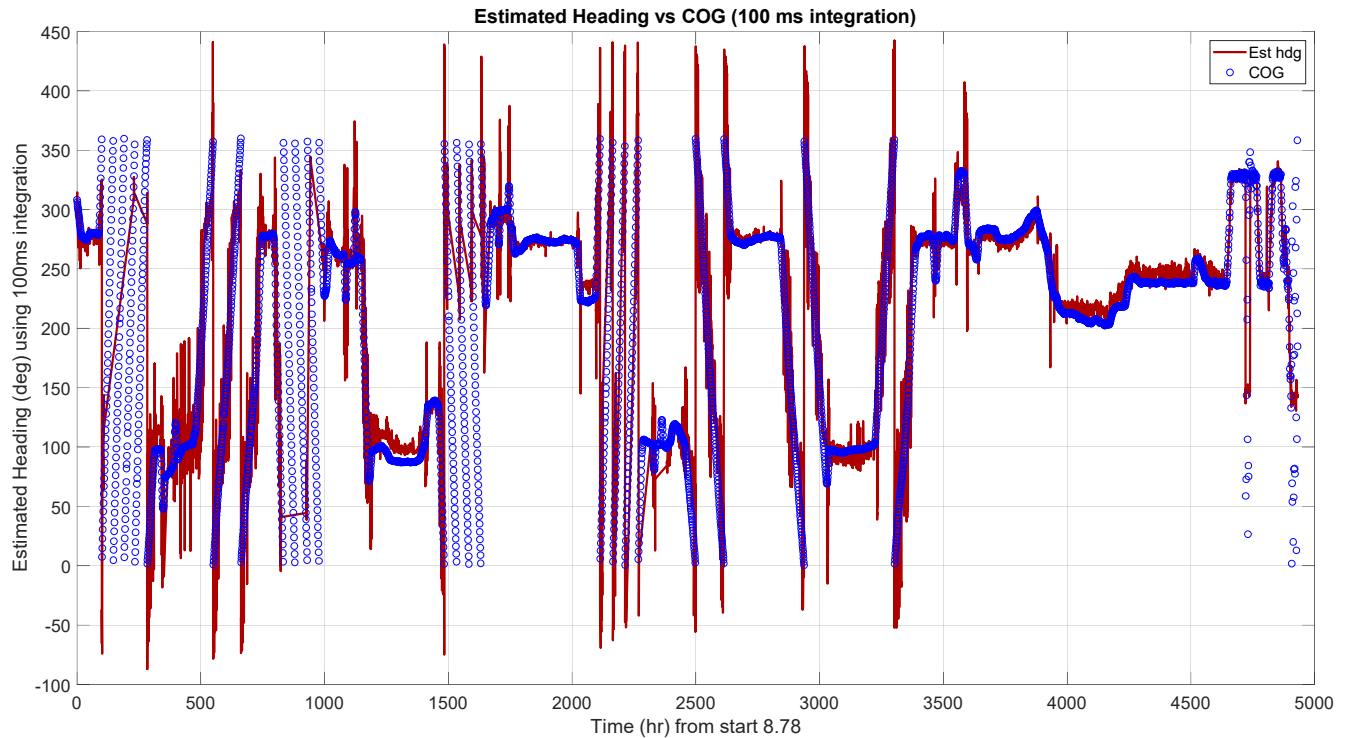


Figure 21. SDR DPA derived heading and GNSS derived Course over Ground (COG) for 2019-09-10; starting 8.78 (8:47 PM)

Table 3. Mean and Standard Deviation (std) of GPS Satellite DOA (in degrees) calculated heading relative to COG (assuming COG is true heading) for segment shown in Figure 19. Filtered LHCP, i.e. only segments where unaided LHCP was tracked, is used (2019-09-09)

| Sat PRN (GPS) | 2 | 12 | 29 | 25 | 31 | 5 |
|---------------|-----|-----|------|-------|------|------|
| Mean (deg) | N/A | N/A | 9.4 | -12.3 | 6.8 | -4.4 |
| Std (deg) | N/A | N/A | 10.4 | 4.7 | 21.3 | 6.8 |

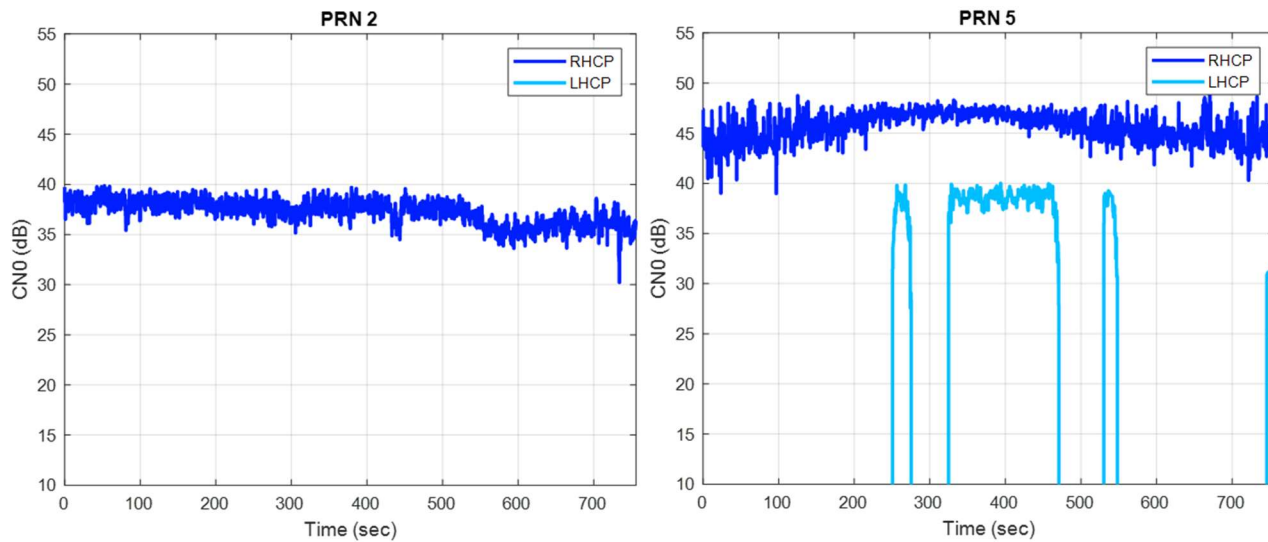


Figure 22. C/N₀ for tracking (unaided) of RHCP and LHCP signal using SDR approach on 2019-09-09

These overall heading estimates help illustrate the benefits and cost of using LHCP phases derived from using RHCP information. Clear benefits are cleaner phases and higher availability of LHCP measurements. In fact, unaided LHCP tracking results in much noisier phases which were not very useful. Instead we examine the use the aided LHCP when we can track the LHCP without aiding (e.g. calculate a C/N₀) which we will call by the shorthand filtered LHCP. This lowers availability as seen in Figure 22 which shows the C/N₀ for unaided RHCP and LHCP tracking. The results for individual heading error satellite heading error with filtered LHCP is shown in Table 3. Lower availability can be also seen in the table. If limited to only periods with COG, PRN 2 and 12 no longer have any measurements. Comparing this table with Table 1, one notices that for the satellites with results, the standard deviation of heading error is lower. This highlights a cost of using the aided LHCP phases without any quality metric – higher error as we may unwittingly use poor quality LHCP measurements resulting in poor DOA estimates. These benefits and drawbacks are evident in Figure 23 and Figure 24 which shows the heading estimate using all available satellites DOA measurements for the all aided LHCP and filtered LHCP, respectively. The aided LHCP has greater availability but more outliers compared to the filtered LHCP. The C/N₀ essentially provides a quality metric to make sure the LHCP phases calculated are not from processing low or no power LHCP with the RHCP tracking results.

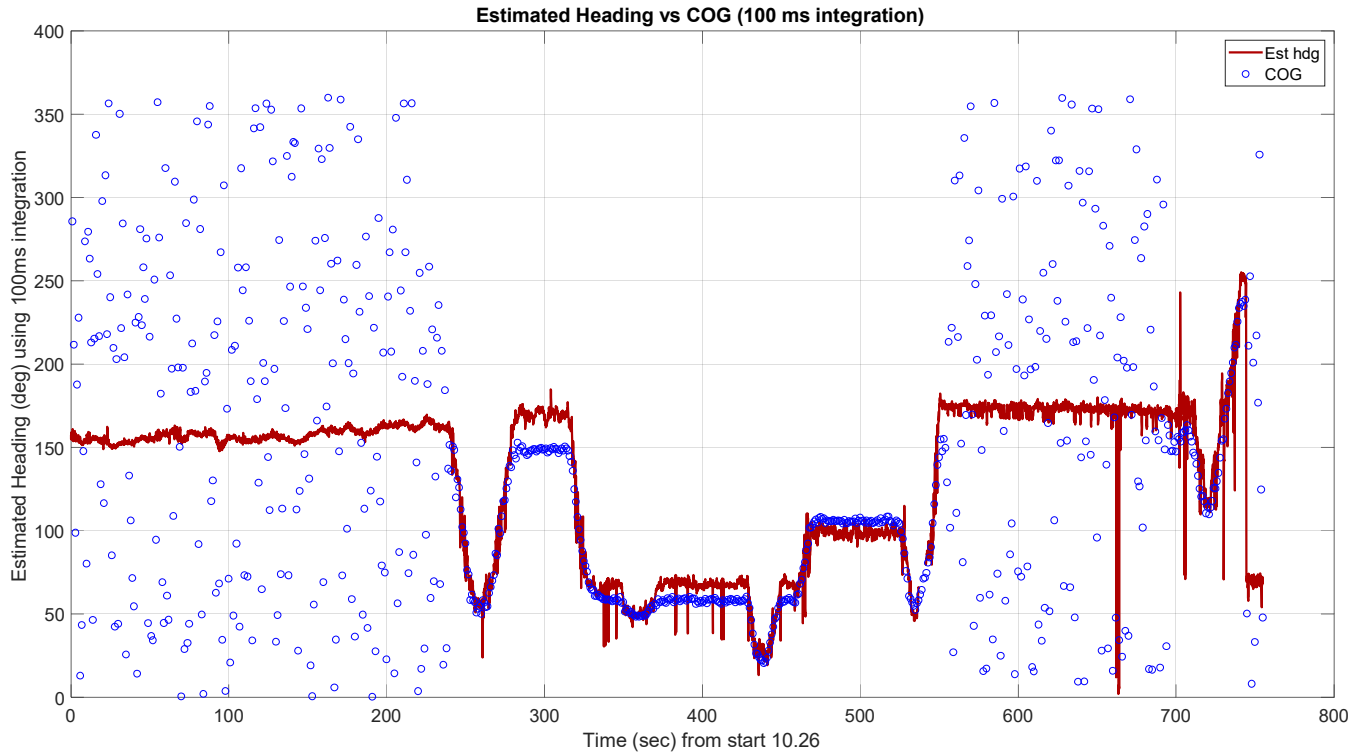


Figure 23. SDR DPA derived heading using aided LHCP phases and GNSS derived Course over Ground (COG) for 2019-09-09; starting 10.26 (10:16 AM)

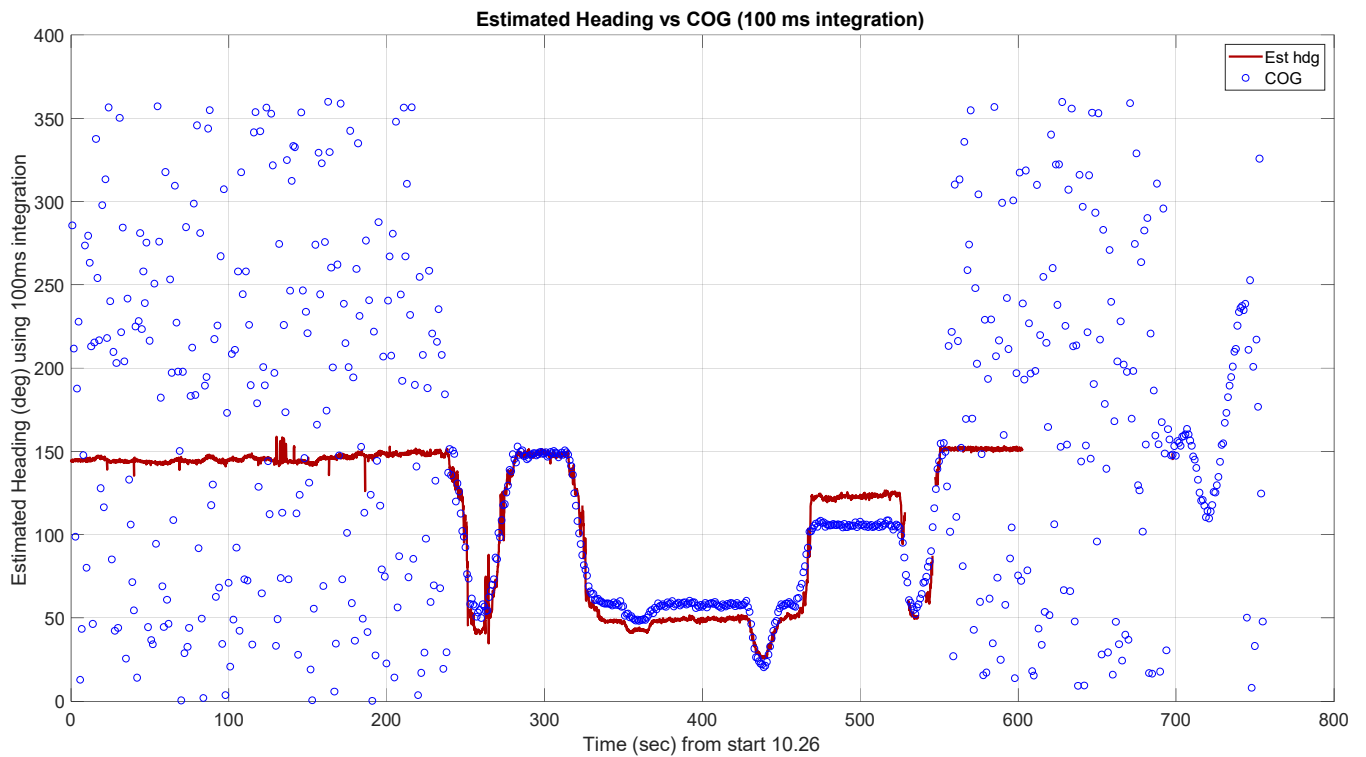


Figure 24. SDR DPA derived heading using aided LHCP phases only if LHCP can be tracked without aiding and GNSS derived Course over Ground (COG) for 2019-09-09; starting 10.26 (10:16 AM)

SUMMARY

The potential of the DPA for spoof detection has now been examined by many groups. Our work focuses on relating the DPA measurement to their physical antecedent – the incoming direction of the signal. This work furthers the development of the technology by demonstrating its ability to measure LHCP and RHCP components and determine DOA on a fast moving (500 kilometers per hour) platform at a high rate.

An improved version of the Stanford PCB DPA was developed and demonstrated to provide rapid DOA estimates of satellite signals allowing for spoof detection and heading determination. The PCB DPA supports two different approaches: one using serial processing using a COTS IC GNSS receiver and a snapshot DOA determination using a SDR. The COTS IC GNSS provided reasonable DOA estimates at 0.5 Hz with typically less than 30 degree standard deviation. Using a software defined radio allowed the DPA to provide azimuth at even faster rate of 10 Hz (even 50 Hz). RHCP tracking aided LHCP phases were demonstrated and used. Care needs to be taken with this architecture and developing good quality metrics for the aided LHCP phases is future work.

We tested the performance of this new DPA in high dynamic flight environment over multiple flights. The on air tests demonstrated improvements in processing speed of DPA DOA for both implementations compared to our previous 50-250 seconds. There is a greater than an order of magnitude improvement in speed which can both better defeat spoofers and enhance DOA measurements through increased averaging. Additional measurements can also aid existing or improve DOA based spoof detection algorithms [14][15][16]. The improved speed limits vulnerabilities that can be exploited by spoofers to defeat the DOA determination.

ACKNOWLEDGMENTS

The authors thank the Federal Aviation Administration (FAA) and the Stanford Center for Position Navigation and Time (SCPNT) for sponsoring this research. The authors also thank the Edwards Air Force Base and the US Air Force (USAF) Test Pilot School providing us with an opportunity to test under representative flight test conditions including open-air GPS jamming. A separate report of the overall flight test program is available from the USAF Test Pilot School (USAF TPS-TIM-19-03). We also thank the USAF 586th Test Squadron for helping test, install and fly our DPA.

The views expressed herein are those of the authors only and are not to be construed as official or those of any other person or organization.

[DISTRIBUTION STATEMENT A. Approved for public release; Distribution is unlimited 412TW-PA-20026]

REFERENCES

- [1] Yu Hsuan Chen, Fabian Rothmaier, Dennis Akos, Sherman Lo, Per Enge, "Towards a Practical Single Element Null Steering Antenna," Proceedings of the Institute of Navigation International Technical Meeting, Monterrey, CA, January 2017
- [2] Yu Hsuan Chen, Fabian Rothmaier, Dennis Akos, Sherman Lo, Per Enge, "Demonstrating Single Element Null Steering Antenna Direction Finding for Interference Detection," Proceedings of the Institute of Navigation International Technical Meeting, Reston, VA, January 2018
- [3] Fabian Rothmaier, Yu-Hsuan Chen, Sherman Lo, J. David Powell, "Single Antenna Heading Estimation," Proceedings of the 32nd International Technical Meeting of the Satellite Division of The Institute of Navigation (ION GNSS+ 2019), Miami, FL September 2019
- [4] Gyles Panther, "Patch Antennas for the New GNSS," GPS World, February 2012, <https://www.gpsworld.com/wirelesspatch-antennas-new-gnss-12552/>

- [5] Matthew Trinkle, W-C Cheuk, "Null-steering GPS dual-polarised antenna arrays" Presented at SatNav 2003 The 6th International Symposium on Satellite Navigation Technology Including Mobile Positioning & Location Services, Melbourne, Australia 22-25 July 2003
- [6] M. Rosen, M. Braasch, "Low-Cost GPS Interference Mitigation Using Single Aperture Cancellation Techniques," Proceedings of the Institute of Navigation National Technical Meeting, 1998 pp. 47-58.
- [7] M. M. Casabona, M. W. Rosen and B. W. Hurley, "Digital interference suppression system for radio frequency interference cancellation". US Patent 5872540, 16 February 1999.
- [8] M. M. Casabona and M. W. Rosen, "Discussion of GPS Anti-Jam Technology," GPS Solution, vol. 2, no. 3, 1999.
- [9] T. Kraus, F. Ribbehege and B. Eissfeller, "Use of the Signal Polarization for Anti-jamming and Anti-spoofing with a Single Antenna," Proceedings of the 27th International Technical Meeting of The Satellite Division of the Institute of Navigation, Tampa, FL, September 2014, pp. 3495-3501.
- [10] Matteo Sgammini, Stefano Caizzzone, Achim Hornbostel, Michael Meurer, "Interference mitigation using a dual-polarized antenna array in a real environment", NAVIGATION, Journal of The Institute of Navigation, Vol. 66, No. 3, Fall 2019, pp. 523-535.
- [11] Emily McMilin, "Single Antenna Null Steering for GPS & GNSS Aerial Applications," Ph.D. Dissertation, Stanford University, March 2016
- [12] Yu-Hsuan Chen, Sherman Lo, Dennis Akos, David De Lorenzo, Per Enge, "Validation of a Controlled Reception Pattern Antenna (CRPA) Receiver Built from Inexpensive General-purpose Elements During Several Live Jamming Test Campaigns," Proceedings of the Institute of Navigation International Technical Meeting Conference, San Diego, CA, January 2013
- [13] Wim De Wilde, Jean-Marie Sleewaegen, Bruno Bougard, Gert Cuypers, Alexander Popugaev, Markus Landmann, Christopher Schirmer, Daniel Egea Roca, José A. López-Salcedo, Gonzalo Seco Granados, "Authentication by Polarization: A Powerful Anti-Spoofing Method," Proceedings of the 31st International Technical Meeting of the Satellite Division of The Institute of Navigation (ION GNSS+ 2018), Miami, FL, September 2018, pp. 3643-3658. <https://doi.org/10.33012/2018.15917>
- [14] Fabian Rothmaier, Yu-Hsuan Chen, Sherman Lo, "Improvements to Steady State Spoof Detection with Experimental Validation using a Dual Polarization Antenna," Proceedings of the 32nd International Technical Meeting of the Satellite Division of The Institute of Navigation (ION GNSS+ 2019), Miami, FL September 2019
- [15] Sherman Lo, Hridu Jain, Yu Hsuan Chen, and Per Enge, "Robust GNSS Spoof Detection using Direction of Arrival: Methods and Practice," Proceedings of the 31st International Technical Meeting of the Satellite Division of The Institute of Navigation (ION GNSS+ 2018), Miami, FL September 2018
- [16] Hridu Jain, Sherman Lo, Yu Hsuan Chen, "Accommodating Direction Ambiguities in Direction of Arrival based GNSS Spoof Detection," Proceedings of Institute of Navigation Pacific PNT, Honolulu, HI, April 2019